Journal of Power Sources 207 (2012) 101–110

Contents lists available at SciVerse ScienceDirect

Journal of Power Sources

journal homepage: www.elsevier.com/locate/jpowsour

Membrane electrode assembly degradation under idle conditions via unsymmetrical reactant relative humidity cycling

S. Vengatesan[a,b], Karachakorn Panha[a], Michael W. Fowler[a,*], Xiao-Zi Yuan[b], Haijiang Wang[b]

[a] Department of Chemical Engineering, University of Waterloo, 200 University Avenue West, Waterloo, ON, Canada N2L 3G1
[b] Institute for Fuel Cell Innovation, National Research Council Canada, 4250 Wesbrook Mall, Vancouver, BC, Canada V6T 1W5

ARTICLE INFO

Article history:
Received 10 August 2011
Received in revised form
19 December 2011
Accepted 20 January 2012
Available online 31 January 2012

Keywords:
Durability
PEM failure modes
RH cycling
Idle condition
Membrane electrode assembly

ABSTRACT

The objective of this study is to investigate membrane electrode assembly (MEA) failure modes under accelerated test conditions via reactant relative humidity (RH) cycling. In this study, the anode and cathode underwent RH cycling in an unsymmetrical manner and the cell was run at a minimal "idle" current during endurance testing. The cell performance was monitored periodically and the degradation curve showed a difference in the anode and cathode induced RH cycling modes. Anode RH cycling had a more pronounced effect on MEA degradation than cathode RH cycling. Electrochemical diagnostic testing methods such as AC impedance and H_2 crossover measurements revealed the degradation phenomena in more detail. The fluoride release data of the anode RH cycling cell showed a sudden increase in fluoride rate within a short period of endurance testing. The infrared imaging results revealed thinning and hotspot pinholes in the membrane, and ionomer delamination from the PTFE reinforcement layer was identified by scanning electron microscopy. The anode RH cycling cell had a shorter lifespan than the cell with cathode RH cycling, highlighting the significance of anode humidification for MEA durability.

1. Introduction

Polymer electrolyte membrane (PEM) fuel cells are a promising energy technology for use in automotive and other portable applications [1,2]. Currently, the cost and durability of fuel cell materials and systems are the major impediments for the successful commercialization of fuel cell technology [3,4]. The reliability of cell materials under diverse operating conditions determines what key materials will be used in fuel cell systems. For automotive applications, fuel cell durability must be targeted in cyclic power output and operational environments [5]. The cyclic power load and operational history of fuel cells is expected to cause changes in the intrinsic properties of cell materials. Changes in the physical and chemical (i.e., morphological and compositional) behavior of the materials impose an overall system efficiency loss. Consequently, designing fuel cell materials that can endure harsh operating conditions is a major challenge for many fuel cell researchers. A detailed understanding of the material failure modes and their mechanisms is therefore essential to assess the reliability of fuel cell materials, and to develop novel or improved materials [6].

Cell components undergo degradation during long-term operation of a fuel cell and stack. Among the types of material degradation, membrane degradation is the main factor shortening the lifetime of PEM fuel cells [7]. Nafion®, an ionomer membrane based on perfluorosulfonic acid (PFSA), is one of the most widely used membranes in fuel cells [8]. In PFSA membranes, the proton conduction mechanism is predominantly associated with water molecules that act as proton carriers. Hence, the desired proton conduction in fuel cell membranes is achieved by sufficiently hydrating the membrane. Insufficient membrane hydration will cause the membrane to dry out, leading to a decrease in proton conduction and an increase in ohmic losses [9,10]. According to Huang et al. [11], low water content in the membrane collapses the crystal structure, which decreases the ion channels and therefore the proton conductivity. Apart from proton conduction, the membrane's mechanical behavior is also strongly affected by the level of membrane hydration [12,13]. Membrane dehydration for longer periods accelerates the rate of membrane degradation and increases the severity of membrane catastrophic failure in the long-term operation of fuel cells [14–17].

Among the several degradation modes [18], membrane mechanical degradation is considered the cause of early failures in fuel cells. Mechanical degradation primarily generates tears, cracks, punctures, or pinholes in the membrane, causing permanent damage [7]. Relative humidity (RH) cycling is viewed as an accelerating tool for membrane mechanical degradation. In practical fuel cell operations, RH cycling will occur during the start-up and shut-down cycles and under cyclic power load conditions. The literature

* Corresponding author. Tel.: +1 888 4567x33415; fax: +1 519 746 4979.
E-mail address: mfowler@uwaterloo.ca (M.W. Fowler).

0378-7753/$ – see front matter © 2012 Elsevier B.V. All rights reserved.
doi:10.1016/j.jpowsour.2012.01.133

contains limited research into the direct consequences of RH cycling on membrane electrode assembly (MEA) degradation [5,19–22]. However, many researchers have studied the mechanical behavior of fuel cell membranes under conditions of cycling humidity and temperature, both experimentally and using numerical models [23–31]. Most of the results revealed the induction of membrane mechanical stresses due to non-uniform swelling of the membrane during hydration cycling. Notably, Kusoglu et al. [27,28] investigated the mechanical response of the membrane under simulated hydration cycling and found that the membrane undergoes plastic deformation due to anisotropic swelling.

In most of the above-mentioned literature, humidity cycling was performed symmetrically on both anode and cathode. However, symmetrical RH cycling induces degradation collectively, making it hard to predict the individual contributions to membrane failure. Although the anode and cathode catalyst layers have the same structures, the electrochemical reactions occurring in the electrodes are quite different. Since the operation history of a fuel cell has a strong impact on its materials, the electrochemical reaction pathways will result in different degradation modes. Identifying the exact cause of failure will provide a more detailed understanding of degradation and its mechanisms [6].

In our previous studies [32,33] this lab investigated MEA failure modes under symmetrical RH cycling conditions and found the membrane mechanical failure mechanism. These studies advanced the development of "diagnostics" for PEM fuel cells, in that failure modes were correlated with in situ performance observations. A change in the rate of voltage degradation was correlated with the formation of pinholes in the membrane. To deepen the knowledge of MEA failure modes, in this work we investigated the influences of anode and cathode RH cycling separately. Accordingly, the RH cycling experiments were performed in an unsymmetrical manner at one side of the fuel cell reactant stream, while keeping the other electrode side fully humidified. The cell was maintained at a very low current density to minimize the impact of chemical degradation associated with operation at open circuit voltage [34,35] based on Wu et al. [36], who investigated fuel cell degradation under idle conditions (close to open circuit) and found membrane-based degradation mechanisms while catalyst-related mechanisms were limited under these conditions. Thus, in the present work, the cell was run under a minimal current (idle current) during accelerated RH cycling testing. An idle current was chosen to eliminate the influence of hydration effects derived from water produced inside the cell, thereby making the cell's hydration entirely controlled by reactant humidification, as well as minimizing chemical degradation of the membrane. Cell performance, cell resistance, membrane crossover, and fluoride release were monitored periodically. The MEA's morphological features and failure locations were identified using scanning electron microscopy (SEM)and infrared (IR) imaging techniques after endurance testing.

2. Experimental

2.1. Membrane electrode assembly and accelerated cell testing

Catalyst coated membranes (CCM, Gore^{TM} 57) were purchased from Gore Primea Inc., and Tandem TP50 cells were used to make single cells with an active area of 42.25 cm^2. The single cells were assembled with the CCM, gas diffusion media (Sigracet®GDL 35BC), bipolar plates, coolant plates, current collectors, and compression end plates. Each assembled single cell was externally pressurized using nitrogen at 110 psi. Hydrogen and air were fed into the anode and cathode at constant flow rate of 0.113 cc min^{-1}, 0.358 cc min^{-1}(during RH cycling experiments) or at the stoichiometry of 1.5 and 2.0 (during polarization measurement), respectively,

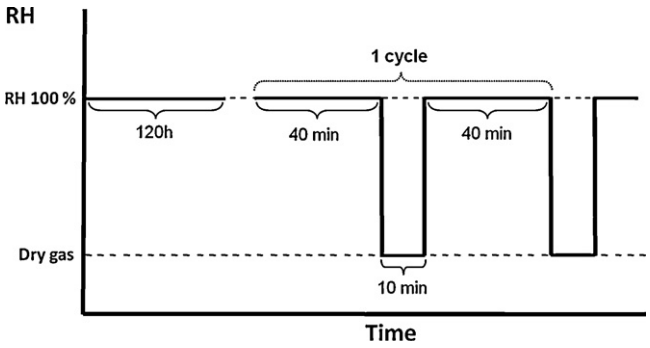

Fig. 1. Schematic diagram of hydration cycling experiments.

with no backpressure on the reactant streams. The cell temperature was maintained constantly at 70 °C by circulating hot water through the coolant plates. The single cell RH cycling profile is shown in Fig. 1. During anode RH cycling, the hydrogen gas was alternated between dry and 100% humidified conditions every 10 and 40 min, respectively. For cathode RH cycling, the air was alternated between dry and 100% humidified conditions for the same time periods. An external modification was made to the experimental setup of a Greenlight G50 test station so that the test station's humidification system was completely bypassed during cycling, and completely dry reactants could be directly fed to the fuel cell. This allowed for rapid (i.e., almost immediate) and complete cycling between RH = 0 and RH = 100 at either the anode or the cathode feed (and the humidification system in the G50 could remain at a steady state for swift return to humidified operation). In both the RH cycling experiments, the opposite electrode was constantly maintained at 100% humidification. During endurance testing, the cell was constantly run at an idle current, i.e., 10 mA cm^{-2}. Although the confounding effects of chemical degradation and catalyst degradation cannot be completely eliminated, "idle" conditions are the least stressful for these modes of aging and membrane degradation.

2.2. Electrochemical testing

The cell performance was monitored periodically by polarization curves using a TDI electronic load box (RBL 232). During the polarization measurement, the anode and cathode were maintained at 100% humidification level. This preconditioning procedure before polarization measurement is used to recover the reversible losses and separate irreversible losses. The hydrogen and air were fed into the anode, cathode at the stoichiometry of 1.5 and 2.0, respectively.

The change in cell resistance was measured by the AC impedance method using a Solartron impedance analyzer (SI 1260) and potentiostat (SI 1286). The potential for the impedance measurements was kept constant at 0.85 V with amplitude of 5 mV. The frequency range used was 10 kHz to 10 mHz. During the impedance testing, the anode and cathode were maintained at 100% humidification level. The hydrogen and air were fed into the anode, cathode at the constant flow rate of 0.113 and 0.358 cc min^{-1}, respectively.

Linear sweep voltammetry (LSV) was carried out using the potentiostat over a voltage range of 0.05–0.6 V with a scan rate of 2 mV s^{-1}. For this, the cathode served as the working electrode, while the anode served as the reference and counter electrodes. During the LSV test, the hydrogen and nitrogen were fed into the anode, cathode at the constant flow rate of 0.1 and 0.3 cc min^{-1}, respectively.

2.3. Fluoride analysis

Water samples were collected from the anode and cathode outlets, and the fluoride content was measured via an ion chromatography method. The water samples were analyzed using an ion chromatograph (Dionex DX 500) with an electrochemical detector (Dionex ED 40). The analytical column used to separate the common anions in the water sample was a Dionex AS17-C plus AG17-C guard column. To carry the anions through the stationary column, 20 mM NaOH buffer solution was used as the mobile phase. The minimum detectable limit of fluoride was 0.011 mg L^{-1}.

2.4. Scanning electron microscopy and infrared imaging

The morphological and interfacial features of the fresh and degraded MEA samples were observed using a scanning electron microscope (Leo1530 SEM). To observe the interfacial features of the MEA, the MEA samples were freeze fractured by immersing in liquid nitrogen, and one half of the sample was mounted upright in the SEM sample holder. IR imaging was used to identify defects or perforations in the degraded MEA. For this, an IR camera (InfraTech GmbH) was used to map the MEA's temperature distribution. The detailed procedure of IR imaging has been described in the literature [37].

3. Results and discussion

As reported earlier [33], to observe the influence of hydration cycling on MEA durability, RH cycling was previously performed in a symmetrical manner on both sides (anode and cathode) of the single cell. During these symmetrical RH cycling experiments, the hydrogen and air were alternated between dry and 100% humidified conditions every 10 and 40 min, respectively. In all the experiments, RH cycling was started after a commissioning period of 120 h, during which the cell was run at 0.6 V. The voltage degradation curve was plotted using the potential versus the cell operation time at a constant current density of 10 mA cm^{-2}. The voltage degradation curve and polarization curves from Ref. [33] are shown here in Fig. 2a and b for comparison with the new experimental results. The degradation curve is separated into three different regions: commissioning, gradual degradation, and highly decayed. The voltage was almost constant during the later stage of commissioning. After the commissioning period, the voltage degradation gradually decreased until 450 h of operation, followed by a rapid decline in cell voltage. This reveals that a significant change in material behavior occurred at this stage in the operating history. As shown in Fig. 2b, the cell performance decreased steadily until 436 h, after which it decreased significantly, especially in the ohmic region. This was mainly attributed to membrane dehydration and proton conductivity loss, due to the insufficient hydration imposed by RH cycling. The cell performance underwent a further rapid decrease at 536 h due to long-term operation of the cell under low membrane hydration, which caused irrecoverable damage to the cell components.

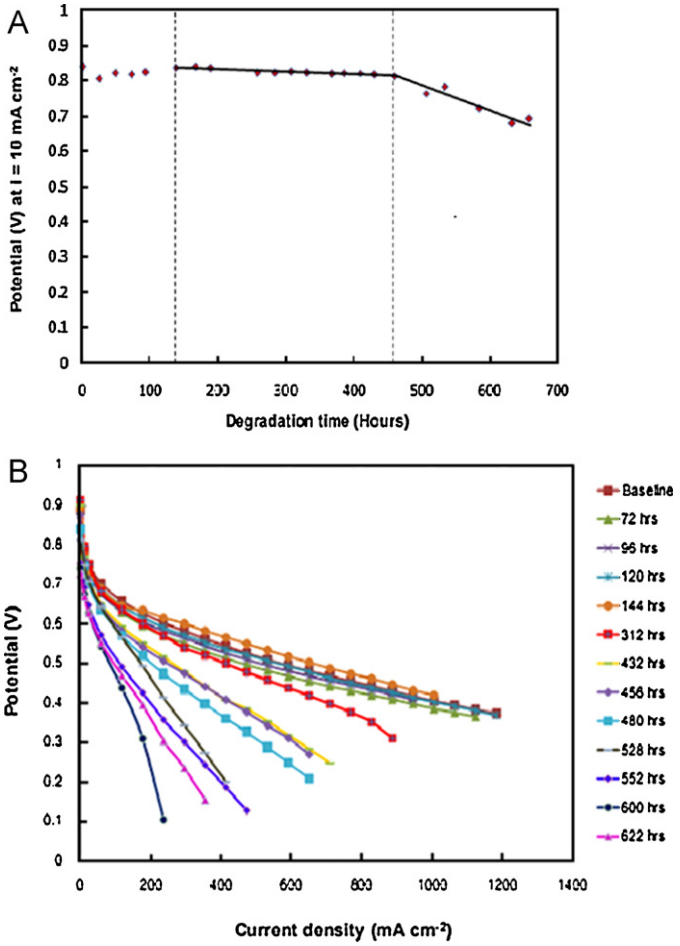

Fig. 2. (a) Voltage degradation curve and (b) *i–V* characteristics of the H_2–air RH cycling cell; T_{cell} = 70 °C; H_2/air stoichiometry = 1.5/2.0, under symmetric RH cycling conditions (i.e., both anode and cathode were dry, then humidified, at the same time). From Ref. [33].

3.1. Effect of anode RH cycling on MEA degradation

In general, during dry fuel cell operation, membrane dehydration mostly occurs at the anode side due to electro-osmotic drag. Under some conditions, back diffusion of water may compensate for water loss on the anode side. The main consequence of dehydration at the anode side is decreased proton conduction and increased ohmic losses[10,38].Since humidification is alternated between wet and dry conditions during anode RH cycling experiments, the anode side will be in a partial dehydration state for some period. During this dehydration state, membrane degradation is expected to be aggravated and accelerated. The degradation curve for anode RH cycling is shown in Fig. 3a. In the commissioning region, there is a continuous decrease in cell voltage, then an increase. In the gradual degradation region, the cell voltage decreases marginally at a degradation rate of 0.2 mV s^{-1}. It may be possible that RH cycling at the anode side caused morphological changes in the catalyst layer, and the catalyst–ionomer interface collapsed. This in turn could have reduced the three-phase boundary and decreased cell performance. However, in the highly decayed region, the cell voltage fluctuates, then decreases drastically at a degradation rate of 0.4 mV s^{-1}. The fluctuations in voltage could have arisen from catalyst layer–membrane delamination or membrane mechanical breaching, as will be presented later in the SEM images. The polarization curves of the anode RH cycling experiments are shown in Fig. 3b. In this case, the anode RH cycling cell completed 100 wet and dry cycles during 440 h of endurance testing. The cell did not show much change in performance until 250 h of operation. However, at 300 h there was a significant decrease in performance, which can be correlated with morphological changes in the catalyst layer and with membrane proton conductivity loss. After 390 h of operation, a rapid decline in the performance curve is noticeable. This decrease may have resulted from irreversible changes in the membrane and catalyst layer, especially at the anode side.

Since impedance tools can reveal changes in material resistance during long-term testing [38], they are highly suitable to indicate the course of material failure modes. Note that the present results

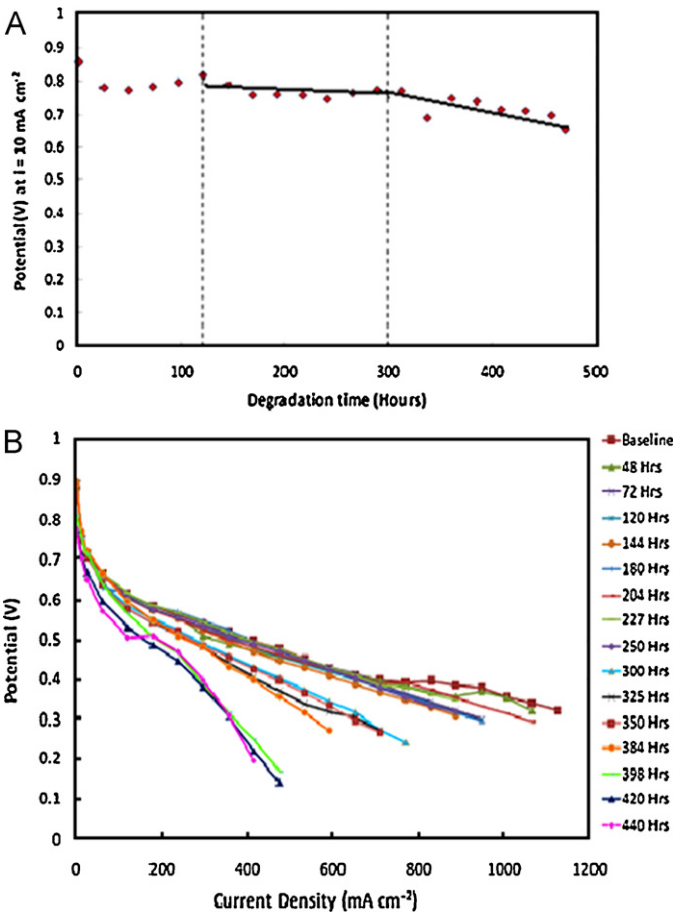

Fig. 3. (a) Voltage degradation curve and (b) *i–V* characteristics of the anode RH cycling cell; T_{cell} = 70 °C; H_2/air stoichiometry = 1.5/2.0.

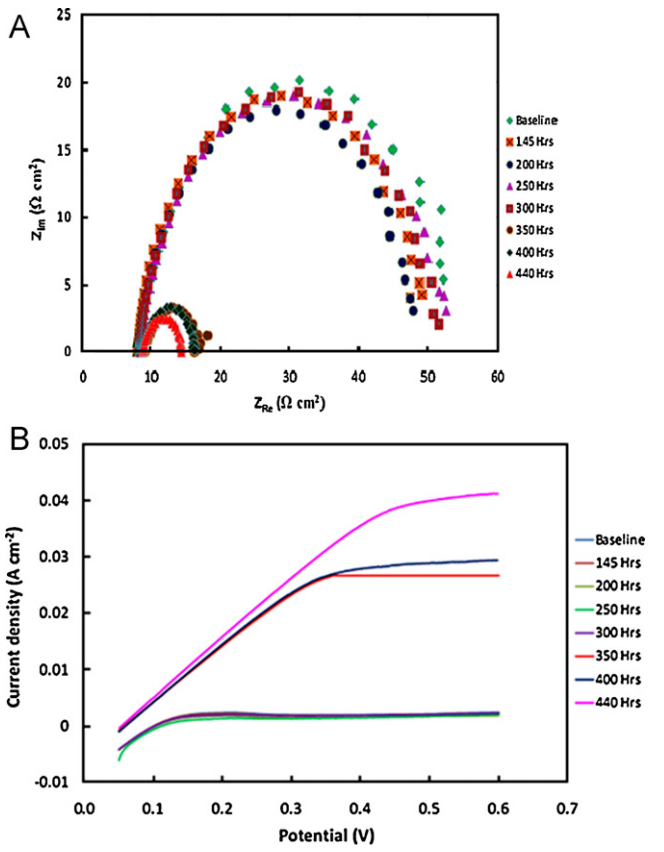

Fig. 4. (a) Impedance spectra of the anode RH cycling MEA at 0.85 V and (b) linear sweep voltammograms of the anode RH cycling MEA; scan rate = 20 mV s^{-1}.

are different from those in Ref. [35], where the accelerated "stress" condition was OCV operation, indicating that a different change in morphology took place in this latest study. The AC impedance spectra of the anode RH cycling cell are shown in Fig. 4a. The cell does not show any significant change in resistance in the high and low frequency regions until 300 h. However, a sharp decrease in the low frequency resistance (LFR) and slight increase in high frequency resistance (HFR) is observable after 350 h of operation. This sudden decrease in LFR might be primarily due to membrane thinning or electrical short formation in the MEA and that will be analyzed with LSV and SEM results in the later section. Also, the slight increase in HFR after 350 h might be attributable to the creep deformation in membrane and electronic conductivity loss due to catalyst layer cracking. Linear sweep voltammetry gives information about the hydrogen crossover current; linear sweep voltammograms are shown in Fig. 4b. It can be seen that the hydrogen crossover current is unchanged until 300 h of cell operation. However, after 350 h there is a sudden increase in crossover current, indicating membrane integrity failure. The abrupt change in crossover current with slight shorting in the limiting current range is observed from the LSV data. This could have arisen from membrane thinning, which accelerates the subsequent membrane degradation process by allowing pinholes to form more easily, as is noticeable from the further increase in hydrogen crossover at the end of the cell life testing. Since the Gore Primea membrane is made with a 3-layer configuration (PTFE layer at the center on which two adjacent ionomer layers are sandwiched), the strong PTFE layer is expected to prevent the gas cross-over. However, the porous PTFE layer can expand to some extent (as can be seen from SEM images, Fig. 6c) during RH cycling and increase the cross-over rate. As the cross-over rate increase dramatically, the membrane failure and pinhole formation also increased. The results from the polarization, impedance analysis, and hydrogen crossover measurements show good agreement, and display a membrane failure mechanism. It is assumed that unsymmetrical RH cycling at the anode side created local stresses and degraded the catalyst layer, leading to delamination of the electrode from the membrane. Since in situ diagnostic tools cannot differentiate between the anode and cathode failure mechanisms, ex situ characterization methods will reveal these failure modes, as will be discussed in later sections.

The anode and cathode water samples were collected separately and analyzed for their fluoride content. Fig. 5a shows the cumulative fluoride ion release over time, revealing that fluoride release increased with time and was higher at the cathode. It is believed that fluoride ions move across the MEA and will be more concentrated at the cathode side due to the electro-osmotic drag process that accompanies water production inside the cell [34]. In addition, the proton would carry the fluoride ion, due to the ion-pair interaction between proton and fluoride ion. As can be seen from the curve, fluoride release was low during the cell commissioning period, and then there was a sudden jump in fluoride release once the RH cycling started at 120 h. The dry anode conditions in this work could have allowed for increased hydrogen crossover, as the pores in the membrane would not have been filled with water. Thus, this work shows that RH cycling causing severe degradation to the ionomer could be due to high gas crossover in dry conditions. According to Liu et al. [39], fluoride release changes with current density, and high fluoride release is found in OCV conditions. Fig. 5b shows the fluoride release rate over time; the rate is irregular and the results are scattered. This can be explained by the change in RH, which leads to alternation in reactant partial pressures and water

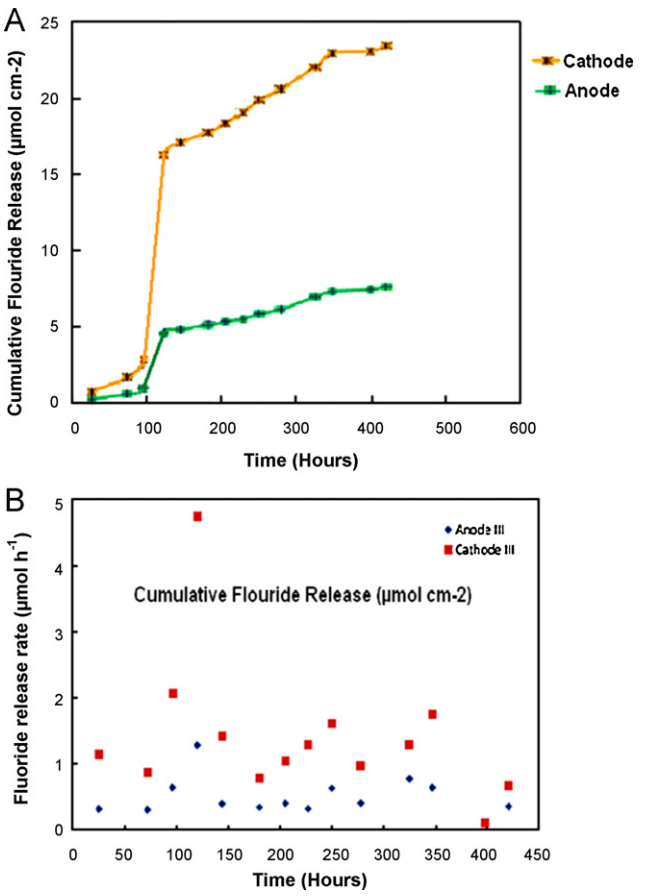

Fig. 5. (a) Cumulative fluoride release and (b) fluoride release rate of the anode RH cycling cell.

management inside the cell. The degradation rate will also change with variations in the RH level, which may create fluctuations in fluoride emission depending on the local water profile in the catalyst layer simply due to there being less water in the cell.

Fig. 6 shows SEM images of fresh and anode RH cycled MEAs. In comparison with the fresh MEA, in the degraded MEA the ionomer layer is slightly detached from the PTFE reinforcement layer, and the PTFE layer is expanded to some extent (Fig. 4c).This may affect the proton transport pathway and may have been responsible for fluctuations in cell performance.

This might have been caused by uneven stresses on the catalyst layer due to RH cycling. Primarily, the anode electrode would expand and contract more than the electrolyte membrane, which would maintain some moisture from the cathode side hydration. Also, it is observed that the membrane (3 layer) thickness of the fresh MEA is changed from 24.8 µm to 23.5 µm in the degraded MEA. By separating the thickness of PTFE layer (center layer) from ionomer layers, the PTFE layer thickness of fresh MEA increased from 5.2 µm to 8.1 µm that confirm the expansion of PTFE layer. However, the ionomer layers thickness is reduced from 19.6 µm to 15.4 µm which show the degradation of ionomer layer during accelerated RH cycling. The surface image of the degraded MEA (Fig. 6d) shows large cracks in the anode catalyst layer at some places, mainly caused by the local stresses from non-uniform water distribution in the catalyst layer during RH cycling. Since the component defects such as cracks, delamination, thickness variations imparted during CCM manufacturing, these small defects would expected to alleviate during the hygro-thermal operation of fuel cells [40].Thus, the large cracks produced can break up the continuity of catalyst layer and thereby increasing the resistance. IR imaging of the fresh and degraded MEAs was carried out after endurance testing, and the results are shown in Fig. 7. Compared with the fresh MEA, the anode RH cycled MEA shows two major hotspot locations. The reason for these locations could be explained as follows: the local stresses created in the membrane due to RH

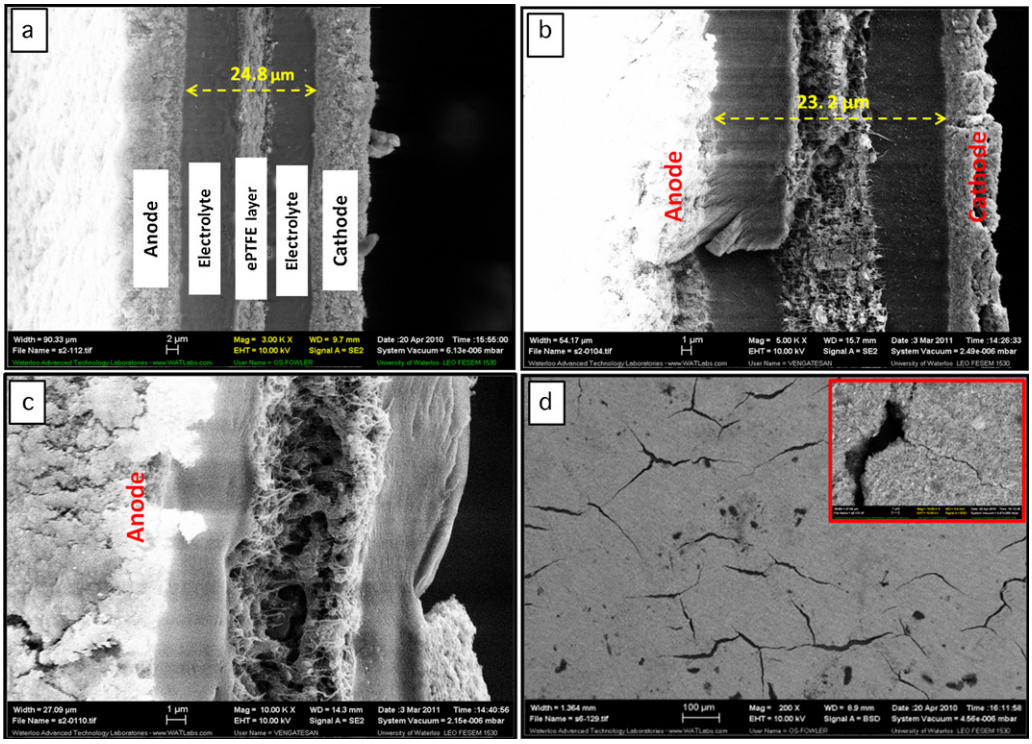

Fig. 6. SEM images of (a) a cross-section of a fresh Gore™ 57 MEA; (b and c) cross-sections of the degraded anode RH cycling MEA; and (d) the surface of the degraded anode RH cycling MEA (inset: magnified view – 10.0K×).

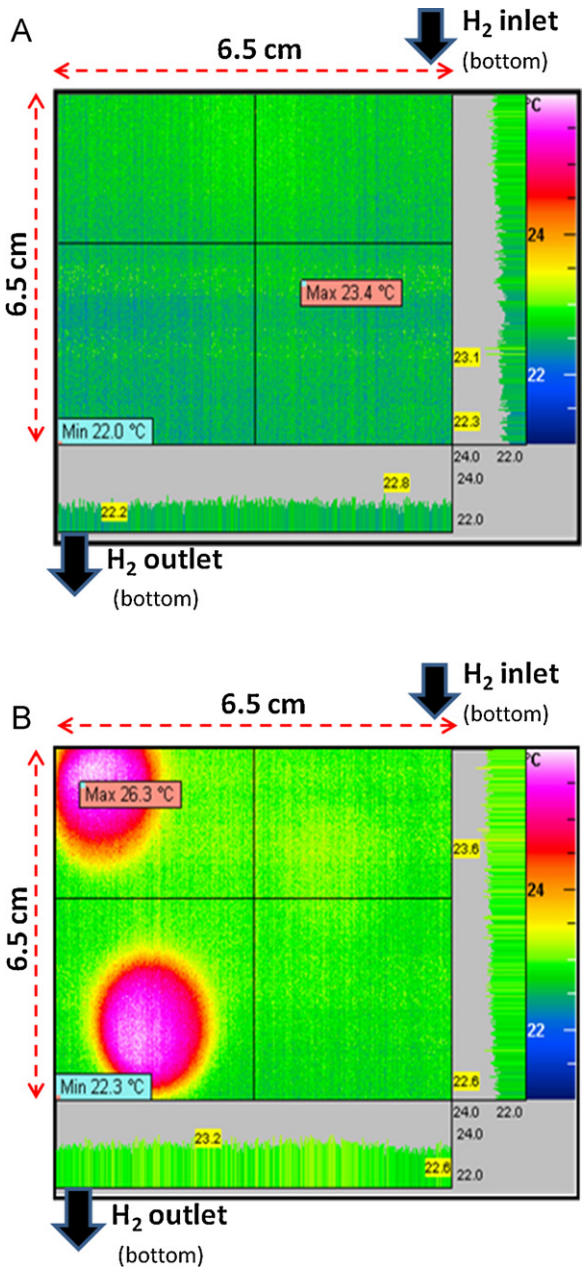

Fig. 7. IR camera images of (a) a fresh Gore™ 57 MEA and (b) the degraded anode RH cycling MEA.

variation cannot be uniform, since the defect sites (cracks, delamination, etc.) present in the pristine Gore MEA may experience high stress and prone to severe damages. These hotspots are expected to have severely increased the crossover current and decreased the lifespan of the membrane during durability testing.

3.2. Effect of cathode RH cycling on MEA degradation

The results of cathode RH cycling exhibit some unique features. Since the electrochemical reaction produces water on the cathode side, RH cycling of the cathode may be expected to have little influence on degradation. Kim et al. [41] studied the effects of cathode inlet RH on MEA durability during start-up/shut-down cycling and found that cycling the cell at low RH values resulted in better durability than at high RH values. In the present study, since the cell was run at a minimal current it was expected to maintain a low RH at the cathode, although some water would be formed. Fig. 8a shows the

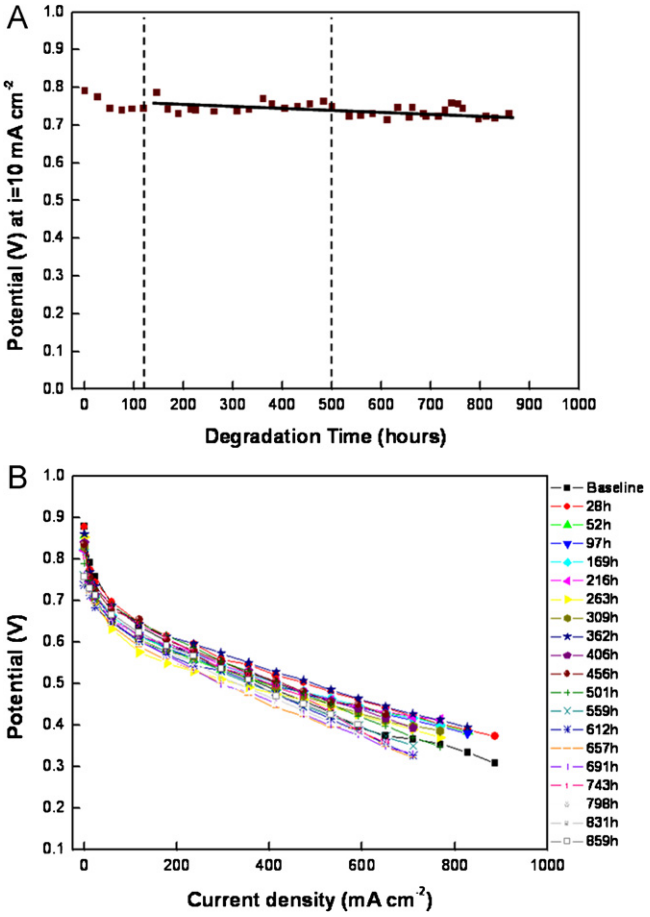

Fig. 8. (a) Voltage degradation curve and (b) polarization curves of the cathode RH cycling cell; T_{cell} = 70 °C; H_2/air stoichiometry = 1.5/2.0.

degradation curve for RH cycling performed only on the cathode side, while keeping the anode at constant 100% humidification. As is clear, the degradation rate is almost steady from the beginning to the end of the cell life, despite the voltage fluctuations. This might reveal that there was no sudden or severe damage to the material structure that would cause the voltage to decrease drastically. However, some reversible material changes occurred, and these might have caused voltage fluctuations due to the overall hydration of the MEA. The reason for these fluctuations will be discussed later. Fig. 8b shows the polarization curves from the RH cycling experiments. The cell performance decreases slowly over time, with no drastic decrease observable until the end of testing, at which point MEA degradation seems to occur via a normal degradation mode.

The AC impedance spectra of the cathode RH cycled cell are illustrated in Fig. 9a. Low frequency resistance increases slightly with operating time, then there is a sharp decrease at 550 h and this continues until the end of cell life. Notably, on the impedance curves both high and low frequency resistances decrease abruptly at 831 h, which differs from the anode RH cycling cell. The decrease in low frequency resistance may be related to the membrane thinning that is evident from the H_2 crossover measurements and IR imaging results. However, the reason for the abrupt decrease in high frequency resistance is still unclear. Fig. 9b presents the linear sweep voltammograms from the cathode RH cycling experiments, showing that the H_2 crossover current density increases slowly and steadily until 686 h.

However, the increase in crossover is well pronounced at nearly the end of life testing, which is probably due to membrane thinning and consequent pinhole formation. Fluoride measurements

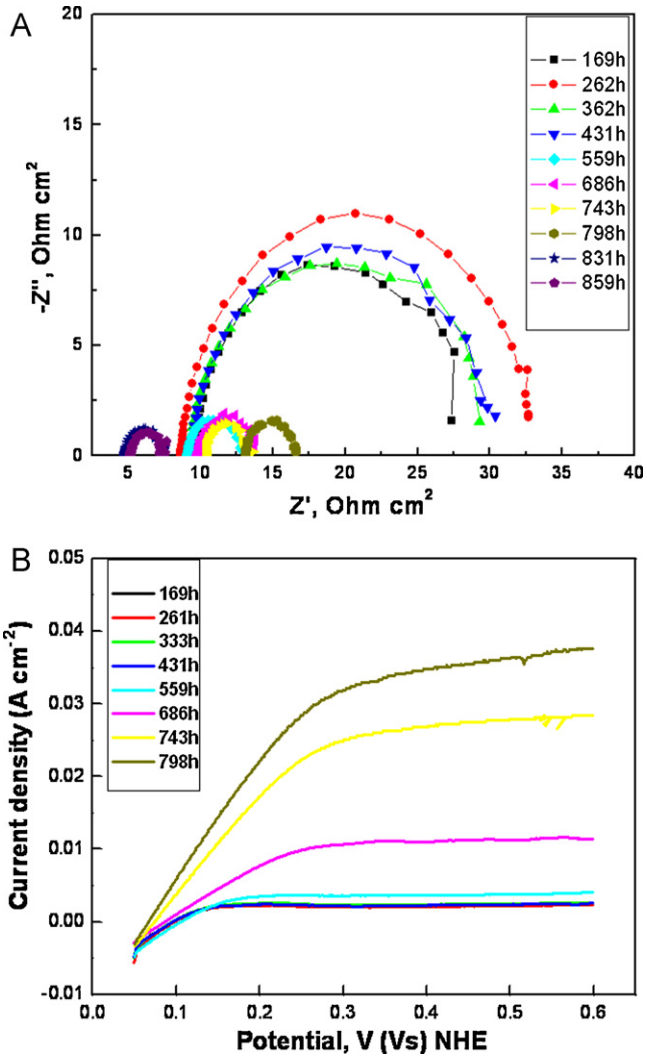

Fig. 9. (a) Impedance spectra of the cathode RH cycling MEA at 0.85 V and (b) linear sweep voltammograms of the anode RH cycling MEA; scan rate = 20 mV s^{-1}.

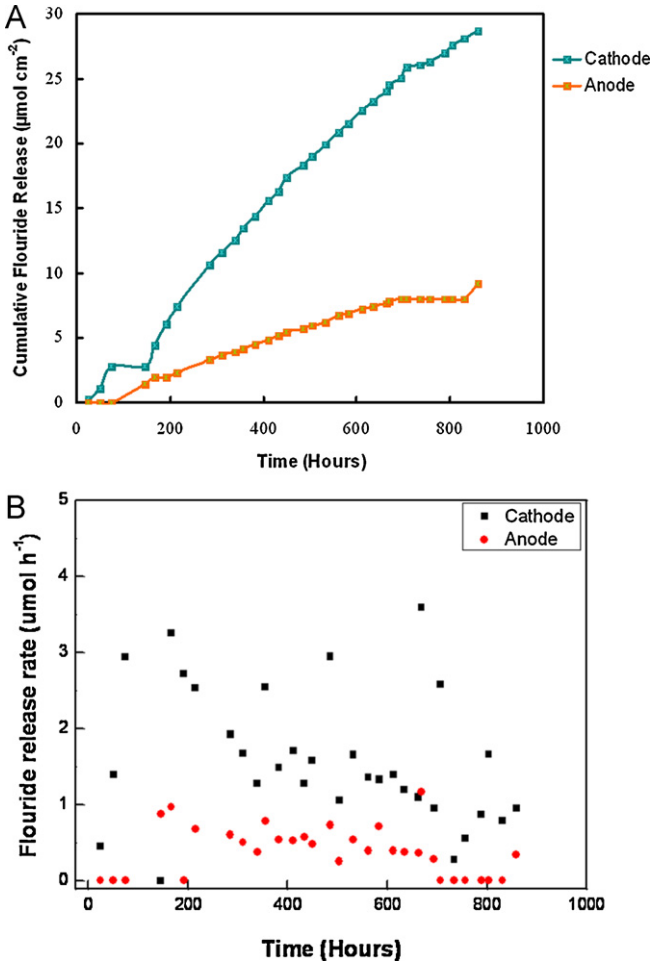

Fig. 10. (a) Cumulative fluoride release and (b) fluoride release rate of the cathode RH cycling cell.

from the collected water samples indicate a steady increase in fluoride release, as shown in Fig. 10. The cumulative fluoride release increases almost linearly, with no abrupt change at any time, which indicates a normal steady membrane degradation mode, likely thinning. Since cathode RH cycling may have a less detrimental degradation effect, the chemical integrity of the ionomer membrane is not abruptly changed.

The morphological features of the MEA were analyzed using SEM and are presented in Fig. 11. In the cross-sectional image of the degraded MEA, the membrane-electrode interface is clearly observable, showing delamination in the membrane layer itself. Generally, Gore™ Primea membranes have a three-layer membrane structure, i.e., ion-conducting electrolytes at either side with a PTFE reinforcement layer in the center, to improve the membrane's mechanical strength. The image reveals that the reinforcement layer is detached from the ionomer layer on both sides. This clearly indicates membrane layer delamination, rather than the common membrane electrode delamination. This could also be a reason for the voltage fluctuation (Fig. 4a) in the cathode RH cycling cell, since the ionomer layer is expected to undergo a continuous lamination/delamination process. In addition, at some locations of the MEA cross-section (Fig. 11b and c) the PTFE layer has completely disappeared, indicating it has been lost. This reveals that the unsymmetrical RH cycling experiment caused membrane delamination by imposing uneven water content across the membrane (more specifically, different hydration in the electrode than in the membrane), and long-term operation of the cell (858 h) allowed for chemical degradation of the PTFE layer. The thickness of the MEA decreased from 24.8 μm (fresh MEA) to 16.0 μm (degraded MEA) and this shows that there was significant thinning of membrane. Besides, the ionomer layer thickness also decreased from 19.6 μm to 12.1 μm. The IR imaging results of the cathode RH cycled MEA after endurance testing are shown in Fig. 12. The temperature profile along the degraded MEA is not uniform, and some high temperature locations are noticeable at the MEA center. These high temperature locations might have resulted from localized PTFE leaching. Nevertheless, the degraded MEA showed overall thinning when compared with the fresh MEA, indicating that when RH cycling was performed only at the cathode, thinning was the predominant failure mode.

3.3. Comparison

Investigating MEA durability using unsymmetrical hydration cycling at the anode and cathode revealed different modes of degradation, depending on which side underwent RH cycling. Under anode RH cycling, MEA performance degraded steadily at the beginning, then showed a rapid decline at the end as pinholes formed. On the other hand, voltage degradation showed a steady decrease from the beginning to the end of endurance testing for the cathode RH cycling cell. The cell performance also gradually declined near the end of the cell life, mimicking normal cell degradation.

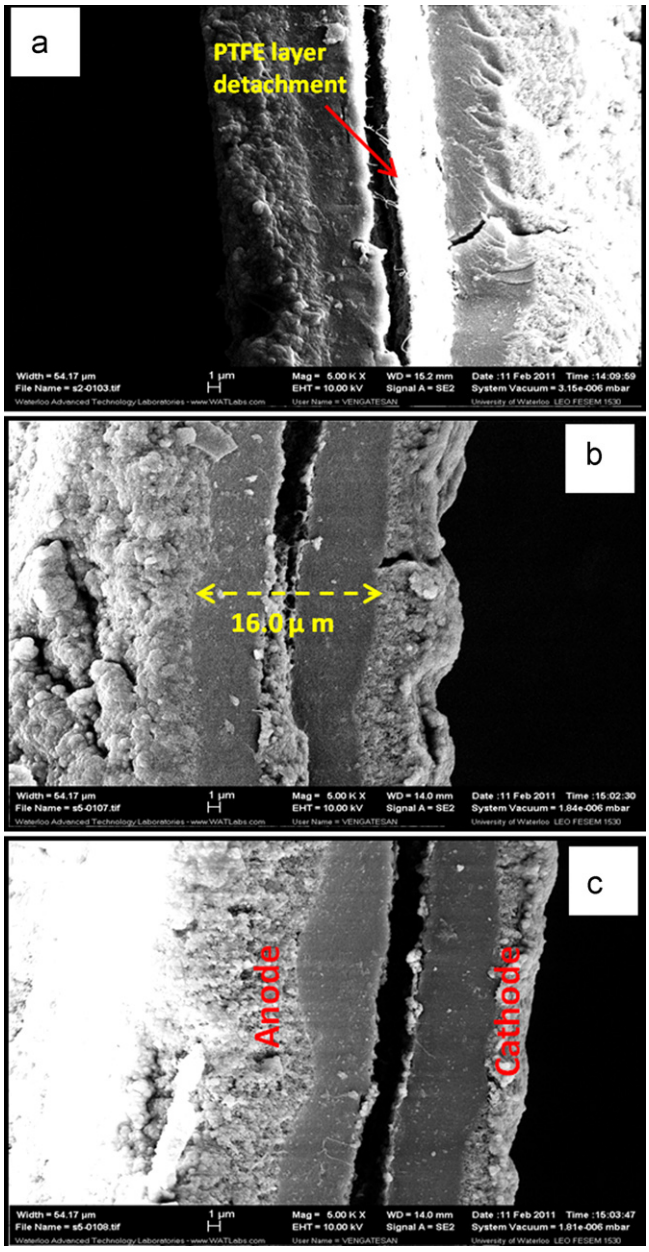

Fig. 11. (a–c) SEM images of cross-sections of the degraded cathode RH cycling MEA.

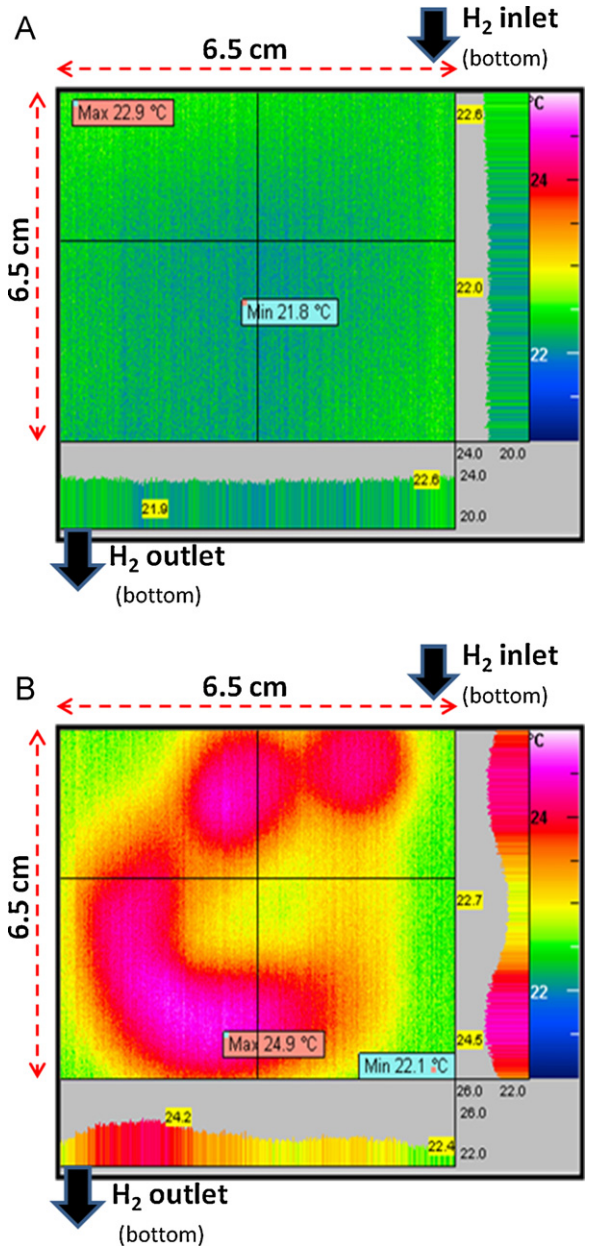

Fig. 12. IR camera images of (a) a fresh Gore™ 57 MEA and (b) the degraded cathode RH cycling MEA.

When compared with symmetrical RH cycling (H_2–air RH cycling) voltage degradation and performance characteristics (Fig. 2a and b), the anode RH cycling cell (Fig. 3a and b) showed similar trends in its performance and voltage degradation. But the cathode RH cycling cell's degradation behavior deviated from that of the H_2–air RH cycling cell.

The impedance results show that the anode and cathode RH cycled cells both exhibited a decrease in high frequency resistance at some stage of operation, likely associated with membrane thinning. In case of anode RH cycling cell, the low frequency resistance drastically decreased within a short operation time due to membrane crazing or pinhole formation from the drying of the anode electrode. In the cathode RH cycling cell this occurred after a longer operation time (559 h), and the two-stage decrease in low frequency resistance of that cell (at 559 h and 831 h) might be attributable to membrane thinning and subsequent leaching of the PTFE layer.

The hydrogen crossover current increased abruptly after 300 h of operation in the anode RH cycling cell, indicating the severity of hydrogen crossover from early pinhole formation when the anode electrode was in a dry condition. It would have been easy for hydrogen molecules to diffuse when the anode catalyst layer and membrane were in a dry state; aside from hydrogen's small size, the pores of the PFSA were not filled with water. In addition, more unreacted hydrogen molecules would have been present because the cell was operated at a very low load, which can increase hydrogen crossover. In the case of the cathode RH cycling cell, hydrogen diffusion into the cathode side was limited due to the completely wet state of the anode catalyst layer and the partially wet nature of the cathode, so the overall MEA was better hydrated.

In the case of the anode RH cycling cell, the cumulative fluoride release was very low during the commissioning period, and then a sudden jump in the fluoride release occurred once the RH cycling started. This indicates that accelerated degradation was induced

by the dry catalyst layer and membrane, due to the attack of OH radicals, which became concentrated (i.e., there was simply less water in the cell). In the case of the cathode RH cycling cell, fluoride release increased gradually and linearly, indicating slower membrane thinning to be the degradation mode. When one compares the cumulative fluoride release values, the anode RH cycling cell showed higher fluoride release at every stage of the endurance testing, which indicates more rapid PFSA degradation overall.

The scanning electron microscopy images show morphological changes in the MEA after endurance testing. In the case of the anode RH cycling cell, cracks in the catalyst layer propagated along the membrane, and partial detachment/delamination of the ionomer layers from the PTFE layer is evident. In the case of the cathode RH cycling cell, the ionomer layer completely detached from the PTFE reinforcement layer, and in some places the PTFE layer vanished. However, this is mainly attributable to longer-term chemical degradation (i.e., the cell being operated for a much longer time). The IR imaging temperature profile shows two major hotspots in the anode RH cycling cell at different locations on the MEA. The cathode RH cycling cell has a more uniform temperature profile, indicating that the more dominant degradation mode was uniform thinning of the membrane over the entire MEA area.

This work has highlighted the different degradation modes that arise in anode or cathode RH cycling cells. From these observations, we can postulate that the uniform membrane thinning in the cathode RH cycling cell resulted in slow degradation and a longer cell lifetime, whereas the uneven thinning and hotspots in the anode RH cycling cell increased the risk of membrane failure, due to non-uniform stress upon the membrane during RH cycling. There are number of literatures that address the issue of water balance and water back diffusion from the cathode to anode [42–44]. To be noted, Yan et al. [42] conducted water mass balance experiments and found that when the anode was maintained at low humidity and low current density while the cathode at 100% humidification level, the best performance was achieved only if the water back diffusion occurred. Based on the above literature, it is apparent that water back diffusion is crucial to operate the fuel cell under dry hydrogen conditions. In our present study, since the cell was operated at very minimal current (10 mA cm^{-2}), it is not expected to have water back diffusion from cathode. Hence, the anode will be more dehydrated in anode RH cycling cell, due to high water drag coefficient and the collapsed catalyst layer. Another reason could be attributed to the high cross-over of oxygen from cathode to dry anode which produces the reactive radical species that degrade the ionomer in the anode catalyst layer. This is evident from the high cumulative fluoride release within short period of cell operation (440 h) in anode RH cycling than cathode RH cycling cell (860 h).

4. Conclusions

A single PEM fuel cell was operated under idle conditions using unsymmetrical RH cycling; the anode and cathode streams underwent cycling separately, the other stream remaining hydrated during the cycling. The cell voltage and performance degradation reveal a difference in the degradation modes for these two RH cycling cells. The anode RH cycling cell exhibits rapid voltage degradation and a shorter lifespan than the cathode RH cycling cell. With anode RH cycling, the membrane resistance increases drastically within a short period of cell operation, and the hydrogen crossover rate also accelerates. The fluoride release of the anode RH cycling cell increases suddenly once the RH cycling experiments starts, indicating the severity of chemical degradation when the catalyst layer undergoes dry operation. The SEM images display cracks in the catalyst layer, as well as the propagation of electrode delamination from the membrane, and the IR imaging results show localized pinhole formation. The cathode RH cycling cell shows gradual voltage degradation, resulting in longer cell endurance. The membrane resistance and hydrogen crossover increase only at the end of cell endurance testing. The cumulative fluoride release increases linearly with time, indicating gradual MEA thinning to be the degradation mode rather than rapid pinhole formation. The morphological features of the MEA reveal a complete delamination of the ionomer layer from the PTFE reinforcement layer. The IR imaging results for the cathode RH cycling cell show almost uniform thinning of the membrane over the entire MEA area.

This study reveals the combined membrane mechanical and chemical failure mechanisms in accelerated humidity cycling conditions, and highlights the role of anode humidification in cell degradation. To improve MEA durability in a RH cycling environment, the operating conditions have to be optimized, and more attention should be given to designing a catalyst layer that better tolerates these harsh conditions, while assuring that some anode stream hydration is maintained.

Acknowledgements

The authors acknowledge the NRC-Helmholtz Joint Research Program and the NRC-University of Waterloo research program for their financial support.

References

[1] S. Srinivasan, R. Mosdale, P. Stevens, C. Yang, Annu. Rev. Energy Environ. 24 (1999) 281–328.
[2] A.J. Appleby, F.R. Foulkes, Fuel Cell Handbook, Van Nostrand Reinhold, New York, 1989.
[3] C. Jaffray, G. Hards, W. in:, A. Vielstich, H.A. Lamm, Gasteiger, Handbook of Fuel Cells, Wiley, New York, 2003.
[4] F.A. de Bruijn, V.A.T. Dam, G.J.M. Janssen, Fuel Cells 8 (2008) 3–22.
[5] X. Huang, R. Solasi, Y. Zou, M. Feshler, K. Reifsnider, D. Condit, S. Burlatsky, T. Madden, J. Polym. Sci. B: Polym. Phys. 44 (2006) 2346–2357.
[6] S. Zhang, X. Yuan, H. Wang, W. Mérida, H. Zhu, J. Shen, S. Wu, J. Zhang, Int. J. Hydrogen Energy 34 (2009) 388–404.
[7] A. Collier, H. Wang, X.Z. Yuan, J. Zhang, D.P. Wilkinson, Int. J. Hydrogen Energy 31 (2006) 1838–1854.
[8] A.B. Laconti, M. Hamdan, R.C.I. McDonald, in: W. Vielstich, A. Lamm, H.A. Gasteiger (Eds.), Handbook of Fuel Cells: Fundamentals, Technology, and Applications, Wiley, England, 2003.
[9] W. Liu, K. Ruth, G. Rusch, J. New Mater. Electrochem. Syst. 4 (2001) 227–231.
[10] Y. Sone, P. Ekdunge, D. Simonsson, J. Electrochem. Soc. 143 (1996) 1254–1259.
[11] C. Huang, K. Seng Tan, J. Lin, K. Lee Tan, Chem. Phys. Lett. 371 (2003) 80–85.
[12] S. Kundu, L.C. Simon, M. Fowler, S. Grot, Polymer 46 (2005) 11707–11715.
[13] M.B. Satterfield, P.W. Majsztrik, H. Ota, J.B. Benziger, A.B. Bocarsly, J. Polym. Sci. B: Polym. Phys. 44 (2006) 2327–2345.
[14] J. Yu, T. Matsuura, Y.M. Yoshikawa, Nazrul Islam, M. Hori, Phys. Chem. Chem. Phys. 7 (2005) 373–378.
[15] J. Healy, C. Hayden, T. Xie, K. Olson, R. Waldo, M. Brundage, H. Gasteiger, J. Abbott, Fuel Cells 5 (2005) 302–308.
[16] S.D. Knights, K.M. Colbow, J. St-Pierre, D.P. Wilkinson, J. Power Sources 127 (2004) 127–134.
[17] E. Endoh, S. Terazono, H. Widjaja, Y. Takimoto, Electrochem. Solid-State Lett. 7 (2004) A209–A211.
[18] P. Rama, R. Chen, J. Andrews, Proc. Inst. Mech. Eng. A: J. Power Energy 222 (2008) 421–441.
[19] C.S. Gittleman, Y.H. Lai, D.P. Miller, AIChE, 2005 Annual Meeting, Cincinnati, Ohio, 2005.
[20] Y.-H. Lai, C.K. Mittelsteadt, C.S. Gittleman, D.A. Dillard, J. Fuel Cell Sci. Technol. 6 (2009) 021002–021013.
[21] T.T. Aindow, J. O'Neill, J. Power Sources 196 (2011) 3851–3854.
[22] M. Crum, W. Liu, ECS Trans. 3 (2006) 541–550.
[23] Y. Tang, A.M. Karlsson, M.H. Santare, M. Gilbert, S. Cleghorn, W.B. Johnson, Mater. Sci. Eng. A 425 (2006) 297–304.
[24] M.N. Silberstein, M.C. Boyce, J. Power Sources 196 (2011) 3452–3460.
[25] R. Solasi, Y. Zou, X. Huang, K. Reifsnider, D. Condit, J. Power Sources 167 (2007) 366–377.
[26] M.N. Silberstein, P.V. Pillai, M.C. Boyce, Polymer 52 (2011) 529–539.
[27] A. Kusoglu, A.M. Karlsson, M.H. Santare, S. Cleghorn, W.B. Johnson, J. Power Sources 161 (2006) 987–996.
[28] A. Kusoglu, A.M. Karlsson, M.H. Santare, S. Cleghorn, W.B. Johnson, J. Power Sources 170 (2007) 345–358.
[29] W. Yoon, X. Huang, J. Power Sources 196 (2011) 3933–3941.

[30] M.F. Serincan, U. Pasaogullari, J. Power Sources 196 (2011) 1303–1313.
[31] D. Bograchev, M. Gueguen, J.-C. Grandidier, S. Martemianov, Int. J. Hydrogen Energy 33 (2008) 5703–5717.
[32] S. Vengatesan, M.W. Fowler, X.-Z. Yuan, H. Wang, J. Power Sources 196 (2011) 5045–5052.
[33] K. Panha, M. Fowler, X. Yuan, H. Wang, Appl. Energy, in press.
[34] S. Kundu, K. Karan, M. Fowler, L.C. Simon, B. Peppley, E. Halliop, J. Power Sources 179 (2008) 693–699.
[35] S. Kundu, L.C. Simon, M.W. Fowler, Polym. Degrad. Stab. 2008 (January), 214–224.
[36] J. Wu, X.Z. Yuan, J.J. Martin, H. Wang, D. Yang, J. Qiao, J. Ma, J. Power Sources 195 (2010) 1171–1176.
[37] S. Zhang, X.Z. Yuan, J.N.C. Hin, H. Wang, J. Wu, K.A. Friedrich, M. Schulze, J. Power Sources 195 (2010) 1142–1148.
[38] J.-M. Le Canut, R.M. Abouatallah, D.A. Harrington, J. Electrochem. Soc. 153 (2006) A857–A864.
[39] W. Liu, M. Crum, ECS Trans. 3 (2006) 531–540.
[40] S. Kundu, M.W. Fowler, L.C. Simon, G. Grot, J. Power Sources 157 (2006) 650–656.
[41] J.H. Kim, E.A. Cho, J.H. Jang, H.J. Kim, T.H. Lim, I.H. Oh, J.J. Ko, S.C. Oh, J. Electrochem. Soc. 157 (2010) B104–B112.
[42] Q. Yan, H. Toghiani, J. Wu, J. Power Sources 158 (2006) 316–325.
[43] Y. Cai, J. Hu, H. Ma, B. Yi, H. Zhang, Electrochim. Acta 51 (2006) 6361–6366.
[44] B. Andreaus, G.G. Scherer, Solid State Ionics 168 (2004) 311–320.